

Multiphoton blockades in pulsed regimes beyond the stationary limits

G. H. Hovsepyan,^{1,2,*} A. R. Shahinyan,^{1,†} and G. Yu. Kryuchkyan^{1,2,‡}

¹*Institute for Physical Researches, National Academy of Sciences,
Ashtarak-2, 0203, Ashtarak, Armenia*

²*Yerevan State University, Alex Manoogian 1, 0025, Yerevan, Armenia*

We demonstrate multiphoton blockades (PB) in the pulsed regime by using Kerr nonlinear dissipative resonator driven by a sequence of Gaussian pulses. It is shown that the results obtained for single-photon, two-photon and three-photon blockades in the pulsed excitation regime differ considerably from analogous results obtained for the case of continuous-wave (cw) driving. We strongly demonstrate that for the case of cw pumping of the Kerr-nonlinear resonator there are fundamental limits on populations of lower photonic number-states (with $n = 0, 1, 2, 3$). Thus, such detailed comparison demonstrates that PB due to excitation with a suitable photon pulses is realized beyond the fundamental limits established for cw excitations. We analyze photon-number effects and investigate phase-space properties of PB on the base of photon number populations, the second-order correlation functions and the Wigner functions in phase space. Generation of Fock states due to PB in the pulsed regime is analysed in details.

PACS numbers:

I. INTRODUCTION

The realization of quantum devices with photon-photon interaction has become an interesting and important research topic in quantum optics and quantum technologies. The key element to obtain the mentioned interactions is strong optical nonlinearity that gives rise to many important quantum effects at level of few-photons, including photon blockade[1–3].

In the photon blockade (PB) the optical response to a single photon is modulated by the presence or absence of the other photons. Particularly, the capture of a single photon into the system affects the probability that a second photon is admitted. Thus, the photon blockade is the analog of the Coulomb blockade for electrons in condensed matter devices, where single electron transport is blocked by a strong Coulomb interaction in a confined structure. A simple consequence of photon blockade is the antibunching of photons in emission in analogy to the photon antibunching of resonance fluorescence on a two-level atom [4, 5].

One of the basic conditions for PB is that the photon-photon interaction strength should be larger regarding decay rate of the system. In this respect, strong nonlinearities on the few-photon level can be produced by interaction between photons and an atom in a cavity [6–9], in systems with interacting photons or polaritons in arrays of cavities coupled to atoms or qubits [10–13], in optomechanical systems and Kerr type nonlinear cavities [14–16].

Photon blockade was first observed in an optical cavity coupled to a single trapped atom [3]. The PB

has been predicted in cavity quantum electrodynamics (QED) [17], and recently in circuit QED with a single superconducting artificial atom coupled to a microwave transmission line resonator [18, 19]. PB was also experimentally demonstrated with a photonic crystal cavity with a strongly coupled quantum dot [20], and was also predicted in quantum optomechanical systems [21, 22]. An analogous phenomenon of phonon blockade was predicted for an artificial superconducting atom coupled to a nanomechanical resonator [23], as well as the polariton blockade effect due to polariton-polariton interactions has been considered in [24]. Recently, PB was considered in dispersive qubit-field interactions in a superconductive coplanar waveguide cavity [25] and with time-modulated input [26].

In most of the cited works PB was considered in nonlinear optical systems driven by a continuous-wave laser. However, photon sources on demand require production of photon pulses at fixed time-intervals. In this paper, we investigate PB in the pulsed regime, considering Kerr-type oscillatory dissipative system driven by a sequence of classical Gaussian pulses separated by time intervals. This approach allows to expand the mechanism of PB for the case of producing few-photon pulses at deterministic time intervals. Thus, we present comparative analysis of one-photon, two-photon and three-photon blockades in the pulsed regimes in addition to the results obtained for the case of PB in cw driving field [16].

In this way, we demonstrate, that contrarily to common expectations, the results obtained in the pulsed regime considerably differ from those derived for the monochromatic driving [16]. More importantly, we see that PB in Kerr-type systems under pulsed excitation can be controlled by shape of pulses. In this spirit, we emphasize the idea of improving the degree of quantum effects in open systems, as well as obtaining qualitatively new quantum effects by applying of the sequence of tailored pulses. This approach was recently exploited for

*gor.hovsepyan@ysu.am

†anna.shahinyan@ysu.am

‡kryuchkyan@ysu.am

formation of high degree continuous-variable entanglement in the nondegenerate optical parametric oscillator [27, 28], and for investigation of quantum interference in mesoscopic domain [29–31]. Recently, generation of nonclassical states in cavity QED with pulsed input has been investigated in [26] and production of a superposition states in the periodically pulsed nonlinear resonator has been demonstrated in [30], [32]. Dynamics of periodically driven nonlinear oscillator has been also studied in the papers [33]– [37].

We clarify the multiphoton photon blockade in Kerr nonlinear resonator under pulsed excitation mainly by considering photon-number effects and by analysing phase-space properties of resonator mode. However, we have not discussed properties of the field transmission when the photons are blocked. Thus, we focus on analysis of the mean photon number, the probability distributions of photons, the second-order correlation functions of photons and the Wigner functions in phase space. In this pulsed regime the ensemble-averaged mean photon numbers, the populations of photon-number states and the Wigner functions are nonstationary and exhibit a periodic time dependent behavior, i.e. repeat the periodicity of the pump laser in an over transient regime. Besides this the results on production of photon Fock states at PB region depend on the parameters of Gaussian pulses such as the amplitude, the duration of pulses and the time-interval between them, dissipation rates and Kerr-interaction coupling. Thus, we investigate production of photonic states for an arbitrary interaction time-intervals including also time-intervals exceeding the characteristic time of dissipative processes, $t \gg \gamma^{-1}$. However, the results obtained are nonstationary that is conditioned by interaction of the system with the sequence of Gaussian e.m. pulses.

For comparison, the paper includes the investigation of the Kerr nonlinear dissipative resonator under cw driving on the framework of the potential solution of the Fokker-Planck equation for the quasiprobability distribution function in complex P-representation. In this way, we obtain that contrarily to the pulsed regime for the case of cw pumping there are fundamental limits on the populations of lower photonic-number-states.

The paper is arranged as follows. In Sec. II we describe periodically pulsed Kerr nonlinear resonator and discuss the case of cw driving in the exact quantum treatment of PB. In Sec. III we consider one-photon, two-photon and three-photon blockades in the pulsed regime on base of the populations of photon-number states and the second-order correlation functions. In Sec. IV we analyse the production of multi-photon states on base of the Wigner functions. We summarize our results in Sec. V.

II. KERR NONLINEAR RESONATOR: PULSED REGIME AND CW LIMIT

The Hamiltonian of Kerr nonlinear resonator under pulsed excitation in the rotating wave approximation reads as:

$$H = \hbar\Delta a^\dagger a + \hbar\chi(a^\dagger)^2 a^2 + \hbar f(t)(\Omega a^\dagger + \Omega^* a). \quad (1)$$

Here, time dependent coupling constant $\Omega f(t)$ that is proportional to the amplitude of the driving field consists of the Gaussian pulses with the duration T which are separated by time intervals τ

$$f(t) = \sum e^{-(t-t_0-n\tau)^2/T^2}, \quad (2)$$

while a^\dagger , a are the creation and annihilation operators, χ is the nonlinearity strength, and $\Delta = \omega_0 - \omega$ is the detuning between the mean frequency of the driving field and the frequency of the oscillator, (see Fig. 1).

This model seems experimentally feasible and can be realized in several physical systems. Particularly, the effective Hamiltonian (1) describes a qubit off-resonantly coupled to a driven cavity. In fact, it is well known that the Hamiltonian of two-level atom interacting with cavity mode in the dispersive approximation, if the two-level system remains in its ground state, can be reduced to the effective Hamiltonian (1). This model also describes a nanomechanical oscillator with a^\dagger and a raising and lowering operators related to the position and momentum operators of a mode quantum motion. An important implementation of Kerr-type resonator has been recently achieved in the context of superconducting devices based on the nonlinearity of the Josephson junction.

We have included dissipation and decoherence in Kerr nonlinear resonator on the basis of the master equation:

$$\frac{d\rho}{dt} = -\frac{i}{\hbar}[H, \rho] + \sum_{i=1,2} \left(L_i \rho L_i^\dagger - \frac{1}{2} L_i^\dagger L_i \rho - \frac{1}{2} \rho L_i^\dagger L_i \right), \quad (3)$$

where $L_1 = \sqrt{(N+1)\gamma}a$ and $L_2 = \sqrt{N\gamma}a^\dagger$ are the Lindblad operators, γ is a dissipation rate, and N denotes the mean number of quanta of a heat bath. To study the pure quantum effects, we focus on the cases of very low reservoir temperatures, which, however, ought to be still larger than the characteristic temperature $T \gg T_{cr} = \hbar\gamma/k_B$. This restriction implies that dissipative effects can be described self-consistently in the frame of the Lindblad Eq. (3). In our numerical calculation we choose the mean number of reservoir photons $N = 0.01$.

Now we describe operational regimes of the system that are relevant to multiphoton blockades. In the absence of any driving, states of the Hamiltonian (1) are the Fock photon states $|n\rangle$ which are spaced in energy $E_n = E_0 + \hbar\omega_0 n + \hbar\chi n(n-1)$ with $n = 0, 1, \dots$. The levels form an anharmonic ladder with anharmonicity that is given by $E_{21} - E_{10} = 2\hbar\chi$.

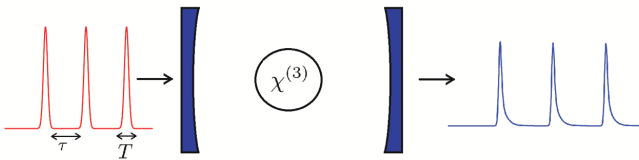


FIG. 1: Schematic representation of Kerr nonlinear resonator under a sequence of Gaussian pulses. In this scheme a emitter involving third-order susceptibility coupled to a resonator.

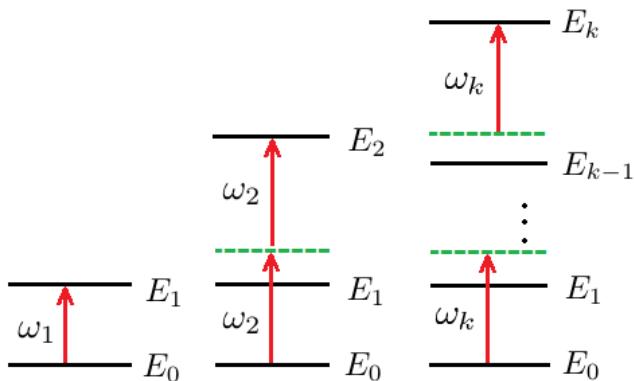


FIG. 2: Schematic energy-level diagram with one-photon, two-photon and k -photon resonant transitions between states of Kerr nonlinear resonator. Selective excitations leading to multiphoton blockades are realized for the main frequencies of driving field: $k\hbar\omega_k = E_{k0}$ that are calculated as $\omega_k = \omega_0 + \chi(k-1)$.

Below, we concentrate on quantum regimes for the parameters leading to resolved oscillatory energy levels. In this case we can consider near the resonant selective transitions between lower photon-number states $|m\rangle \rightarrow |n\rangle$. In this way, k -photon blockades for the positive $k = 0, 1, 2, 3, \dots$ are realized in both resonant and near the resonant transitions between oscillatory initial and final states $|0\rangle \rightarrow |k\rangle$. According to the formula $E_n = E_0 + \hbar\omega_0 n + \hbar\chi n(n-1)$ the resonant frequencies of these transitions equal to $k\hbar\omega_k = E_{k0}$ and can be derived in the following form $\omega_k = \omega_0 + \chi(k-1)$ (see, Fig. 2). Thus, for one-photon transition $k = 1$ and $E_{10} = \hbar\omega_0$, the resonance frequency is $\omega_1 = \omega_0$, for two-photon transition $k = 2$ and $E_{20} = 2\hbar\omega_0 + 2\chi$, the other resonance frequency is $\omega_2 = \omega_0 + \chi$, while for $k = 3$, $E_{30} = 3\hbar\omega_0 + 6\chi$, the resonance frequency is $\omega_3 = \omega_0 + 2\chi$.

Considering the pulsed regimes of Kerr nonlinear reservoir we assume that the spectral pulse-width, i.e. the spectral widths of pulses, should be smaller than the nonlinear shifts of the oscillatory energy levels. It means that the duration of pulses should be larger than $1/\chi$. Thus, for strong nonlinearities $\chi/\gamma > 1$, we arrive to the following inequalities for the duration of Gaussian pulses $1/\gamma > T > 1/\chi$.

We solve the master equation Eq. (3) numerically

based on quantum state diffusion method. The applications of this method for studies of NDO can be found in [29]-[32]. In the calculations, a finite basis of number states $|n\rangle$ is kept large enough (where n_{max} is typically 50) so that the highest energy states are never populated appreciably. In the following the distribution of oscillatory excitation states $P(n) = \langle n|\rho|n\rangle$ as well as the Wigner functions

$$W(r, \theta) = \sum_{n,m} \rho_{nm}(t) W_{mn}(r, \theta) \quad (4)$$

in terms of the matrix elements $\rho_{nm} = \langle n|\rho|m\rangle$ of the density operator in the Fock state representation will be calculated. Here (r, θ) are the polar coordinates in the complex phase-space plane, $x = r \cos \theta$, $y = r \sin \theta$, whereas the coefficients $W_{mn}(r, \theta)$ are the Fourier transform of matrix elements of the Wigner characteristic function.

In this way, we calculate below nonstationary representation of a single emitter coupled to an optical resonator populations P_0, P_1, P_2, P_3 of photon-number states $|n\rangle$, $n = 0, 1, 2, 3$, as well as the mean photon number, the Wigner functions and the second-order correlation functions.

A. Limits to the state populations for the case of cw driving

In this subsection we shortly discuss selective excitation of a Kerr nonlinear resonator under cw driving. In this case the Hamiltonian (1) reads as:

$$H = \hbar\Delta a^\dagger a + \hbar\chi(a^\dagger)^2 a^2 + \hbar(\Omega a^\dagger + \Omega^* a), \quad (5)$$

i.e. describes a standard anharmonic oscillator driven by a monochromatic field in the rotating wave approximation. In this simplest case, an analytical results for a dissipative driven nonlinear oscillator in steady state have been obtained in terms of the solution of the Fokker-Planck equation for the quasiprobability distribution function $P(\alpha, \alpha^*)$ in complex P-representation [38]. This approach based on the method of potential equations leads to the analytic solution for the quasiprobability distribution function $P(\alpha, \alpha^*)$ within the framework of an exact nonlinear treatment of quantum fluctuations. In this way, the photon number probability distribution function $p(n) = \langle n|\rho|n\rangle$ can be expressed in terms of complex P-representation as follows:

$$p(n) = \frac{1}{n} \int \int_C d\alpha d\alpha^\dagger (\alpha)^n (\alpha^\dagger)^n \exp(-\alpha\alpha^\dagger) P(\alpha, \alpha^\dagger), \quad (6)$$

where C is an appropriate integration contour for each of the variables α and α^* , in the individual complex planes. After integration the mean photon number and the probability distribution of photon-number states are repre-

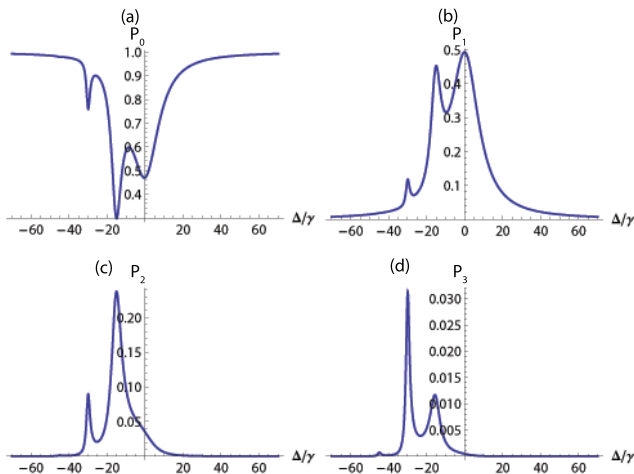


FIG. 3: Populations of photon number depending on the detuning. The parameters are: $\Omega/\gamma = 20$, $\chi/\gamma = 15$.

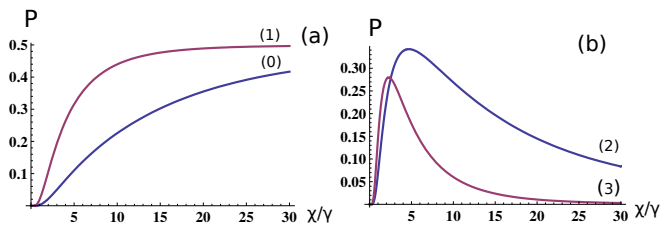


FIG. 4: Populations of photon numbers depending on the parameter of nonlinearity: the curves of P_0, P_1 populations (a), the curves of P_2, P_3 populations (b). The parameters are: $\Omega/\gamma = 20$, $\Delta/\gamma = 0$.

sented in the following form [39–41]:

$$\langle a^\dagger a \rangle = \frac{\Omega^2}{(\Delta + \chi)^2 + (\gamma/2)^2} \frac{F(\lambda + 1, \lambda^* + 1, z)}{F(\lambda, \lambda^*, 2|\varepsilon|^2)}, \quad (7)$$

where $\varepsilon = \Omega/\chi$, $\lambda = (\gamma + i\Delta)/i\chi$, and $F = {}_0F_2$ is the hypergeometric function:

$${}_0F_2(a, b, z) = \sum_{k=0}^{\infty} \frac{z^k \Gamma(a) \Gamma(b)}{k! \Gamma(k+a) \Gamma(k+b)}, \quad (8)$$

$$P(n) = \frac{|\varepsilon|^{2n} \Gamma(\lambda) \Gamma(\lambda^*)}{n! {}_0F_2(\lambda, \lambda^*, 2|\varepsilon|^2)} \sum_{k=0}^{\infty} \frac{|\varepsilon|^{2k}}{k! \Gamma(k+n+\lambda) \Gamma(k+n+\lambda^*)}. \quad (9)$$

In Fig. 3 we present the typical results for the populations P_0, P_1, P_2, P_3 of the photon-number states $|n\rangle$ versus the detuning that are calculated on the Eq. (9). These results show the selective excitations of the Fock states $|1\rangle, |2\rangle, |3\rangle$. As we see, the population P_1 depicted in Fig. 3(b) displays the maximum 0.5 at $\Delta = 0$, that corresponds to the resonance transition $|0\rangle \rightarrow |1\rangle$ at the frequency $\omega = \omega_0$. The other maximum $P_1 = 0.46$ at $\Delta/\gamma = -15$ corresponds to the population of $|1\rangle$ state

through the Raman process with the energy conservation $E_0 + 2\omega_2 = \omega_k + E_1$. This process involves the excitation of Fock state $|2\rangle$, (in the transition $|0\rangle \rightarrow |2\rangle$) at the frequency of pump field $\omega_2 = \omega_0 + \chi$, and the decay $|2\rangle \rightarrow |1\rangle$ at frequency $\omega_k = \omega_0 + 2\chi$. Note, that the population of vacuum state is zero in this spectral range (see, Fig. 3(a)). The population P_2 depicted in Fig. 3(c) displays the maximum 0.24 at $\Delta = -15$, that corresponds to the resonance transition $|0\rangle \rightarrow |2\rangle$ at the frequency $\omega = \omega_0 + \chi$. As we see, the population P_3 is very small for all values of the detuning. Nevertheless, the population display maximum at $\Delta/\gamma = -30$. This peak corresponds to three quanta excitation of $|3\rangle$ state at the frequency $\omega_3 = \omega_0 + 2\chi$.

In general, from the analytic results and numerical analysis we can conclude that the populations are strongly limited. We demonstrate this fact in Fig. 4 by showing the dependence of populations from the parameter of nonlinearity. We observe in Fig. 4(a) that both populations of vacuum and single-photon states monotonically increase with increasing of the nonlinearity parameter. However, the population P_1 is limited by the value 0.5. This effect of selective excitation can be interpreted as the single-photon Fock state blockading the generation of two or more photons. However, limit to P_1 population is restricted possibility of observation PB in cw regime. Note, that this result is in accordance with the numerical results observed on framework of the master equation [16]. The behavior of the populations of two-photon and three-photon number states depicted in Fig. 4(b) differ from P_0 and P_1 . We observe that these populations display peaked structures and the maximum are realized for the definite parameters of nonlinearity.

One of the questions that we will try to answer below is whether or not the populations P_n of $|n\rangle$ states for Kerr nonlinear dissipative resonator driven by a sequence of Gaussian pulses can exceed the cw limits.

III. PB IN THE PULSED REGIMES

Now we present the results of this paper concerning selective excitations of photon-number states and hence the observation of an effective PB due to pulsed excitation. In this sense, we note the main peculiarity of our paper. We investigate photon-number aspects of PB in nonstationary regimes, for an arbitrary interaction time intervals, that also can exceed the characteristic time of dissipative processes, $t \gg \gamma^{-1}$. These nonstationary regimes are conditioned by the specific form of excitation.

If the Kerr nonlinear resonator is driven by a sequence of pulses, its behavior is modified and essentially depends from the duration of pulses as well as time-intervals between them. In this way, we consider three important regimes leading to one-photon, two-photon and three-photon blockades. In these regimes the production of single-photon, two-photon- and three-photon states blockade the generation of the other photons. Each

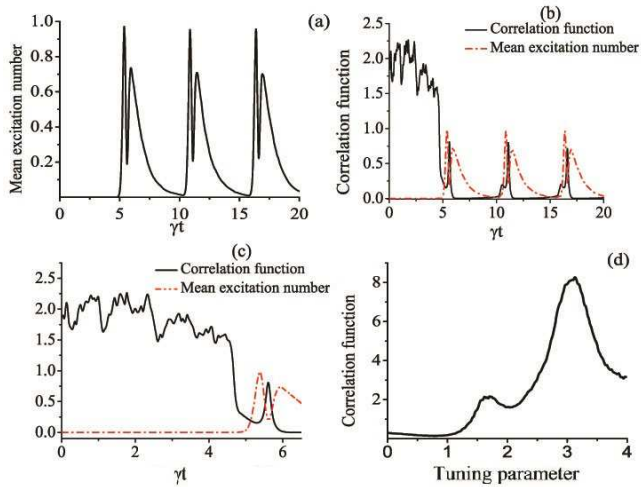


FIG. 5: The regime of single-photon blockade. The mean photon number versus time-interval that repeats the Gaussian pulses and also indicates decay effects, for $k = 1$ (a); the time-evolution of the second-order photon correlation function versus the dimensionless time, for $k = 1$ (b),(c); the second-order photon correlation function, for time-intervals at the peak values of the mean photon numbers, versus the tuning parameter (d). The parameters are: $\chi/\gamma = 15$, the maximum amplitude of the driving field $\Omega/\gamma = 6$, the mean number of reservoir photons $N = 0.01$, $\tau = 5.5\gamma^{-1}$, $T = 0.4\gamma^{-1}$.

of these regimes are realized for the appropriate choosing parameters, the detuning Δ , the nonlinearity parameter χ , the pump amplitude Ω and the parameters of pulses. Note, that in the case of pulsed excitation the ensemble-averaged mean oscillatory excitation numbers and the populations of oscillatory states are nonstationary and exhibit a periodic time dependent behavior, i.e. repeat the periodicity of the pump laser in an over transient regime. Below we demonstrate that the concrete PB regimes can be effectively prepared if the pulsed excitation is tuned to the corresponding resonance transitions. For convenience, we shall refer to k as a tuning continuous parameter instead of the detuning Δ . Thus, by choosing the concrete value of tuning parameter k in the expression $\omega_k = \omega_0 + \chi(k-1)$ we determine the detuning.

The other conditions to improve the effectiveness of PB concern to choosing the controlling parameters of the pulses. We assume the regimes involving short pulses separated by long time intervals that allow to increase the weights of photon-state populations.

A. One-photon blockade

The analysis of the master equation Eq. (3) shows single-photon blockade in Fig. 5 and Fig. 6. In this regime, the probability distribution of excitation numbers $P(n)$ displays maximum, approximately equals to unity for single-photon state, $n = 1$, for the tuning pa-

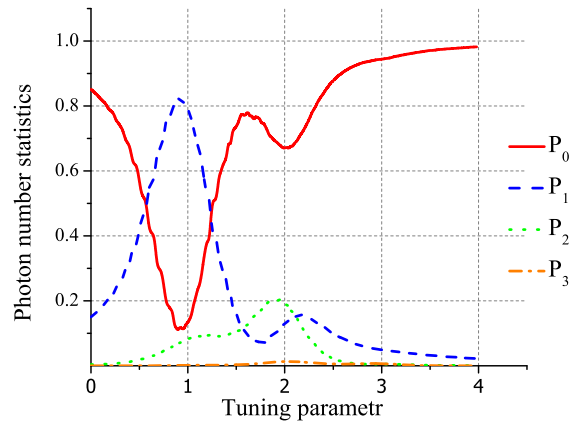


FIG. 6: The regime of single-photon blockade. The populations $P(n)$ of $|n\rangle$ Fock states, for $n = 0, 1, 2, 3$, at the maximal peak values of the mean photon numbers, versus the tuning parameter. The parameters are: $\chi/\gamma = 15$, the maximum amplitude of the driving field $\Omega/\gamma = 6$, the mean number of reservoir photons $N = 0.01$, $\tau = 5.5\gamma^{-1}$, $T = 0.4\gamma^{-1}$.

rameter $k = 1$ or the detuning $\Delta = 0$. We also analyze the populations of photonic states for the definite time-intervals corresponding to the maximal peak values of the mean photon numbers according to Fig. 5(a). The values of populations at these peaks versus the tuning parameter are depicted in Fig. 6. As we see, for the parameters: $\chi/\gamma = 15$, $\Omega/\gamma = 6$, $\tau = 5.5\gamma^{-1}$, and $T = 0.4\gamma^{-1}$ the maximum of $|1\rangle$ Fock state population reaches to $P_1 = 0.82$ approximately for $k = 1$, i.e. for the near to resonance frequency $\omega_1 = \omega_0$. In this case the populations of the other states are very small, particularly, P_0 of vacuum state is approximately equals to 0.14 and P_2 of $|2\rangle$ Fock state is 0.04.

It is interesting to compare these results with the solutions obtained for the Kerr nonlinear resonator with cw driving field. It has been shown numerically [16] that in the case of cw-excitation the maximum rate of the population P_1 reach only to 0.5 for $k = 1$ and approximately equals to the population of vacuum state P_0 . The limit 0.5 for P_1 has been also obtained by analytical calculations in the previous section. Thus, the population $P_1 = 0.82$ calculated in the pulsed regime essentially exceeds the analogous result in cw regime. This result indicates the efficiency of the single-photon blockade in the pulsed regime. Indeed, we can conclude that such high population of single-photon state effectively blockades the entering of the other photons in the resonator.

To observe photon blockade we also turn to calculation of the normalized second-order correlation function for zero delay time $g^{(2)}$ that is defined as:

$$g^{(2)}(t) = \frac{\langle a^\dagger(t)a^\dagger(t)a(t)a(t) \rangle}{(\langle a^\dagger(t)a(t) \rangle)^2}. \quad (10)$$

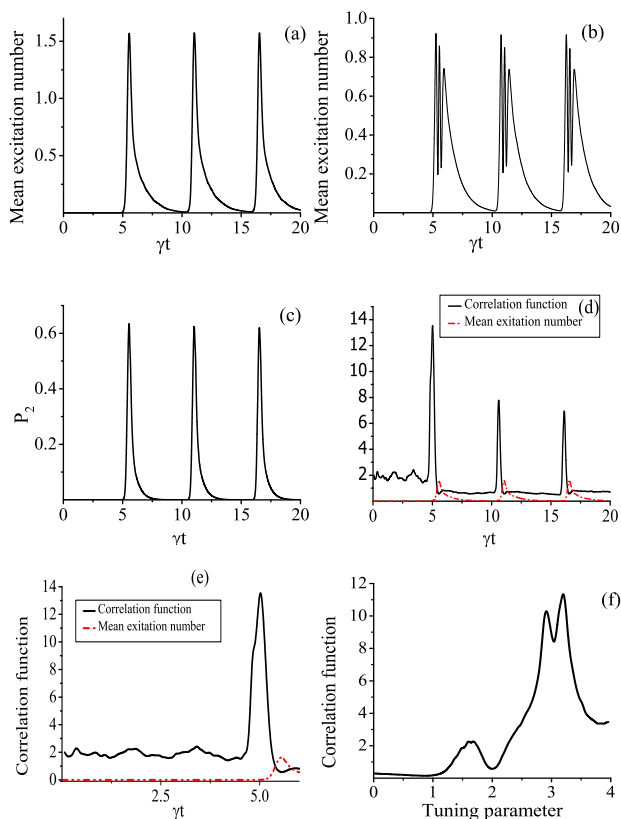


FIG. 7: The regimes of single-photon and two-photon blockades. The mean photon numbers versus dimensionless time-interval for $k = 2$ (a) and $k = 1$ (b) that repeat the Gaussian pulses and involve also decay effects; time-evolution of the population P_2 of $|2\rangle$ Fock state, for $k = 2$, versus dimensionless time (c); the second-order photon correlation function versus the dimensionless time, for $k = 2$ (d), (e); the second-order photon correlation function for time-intervals at the peak values of the mean photon numbers versus the tuning parameter (f). The parameters are: $\chi/\gamma = 30$, the maximum amplitude of pump field $\Omega/\gamma = 12$, the mean number of reservoir photons $N = 0.01$, $\tau = 5.5\gamma^{-1}$, $T = 0.4\gamma^{-1}$.

The results are depicted in Fig. 5(b, c, d). The non-stationary correlation function versus dimensionless time intervals is shown in Fig. 5(b) with the curve of mean photon number, while the result describing the photon correlation for short time intervals is presented in Fig. 5(c). As we see, for short time intervals $t = (0 - 5)\gamma^{-1}$ only thermal cavity photons are involved and the time dependence of $g^{(2)}(t)$ in this area describes photon correlation of thermal bath at the averaged level $g^{(2)} = 2$. During the pulses, if P_1 reach to the maximum, the probability of generation of a second photon is suppressed. In this case oscillatory mode acquired sub-poissonian statistics with the second-order correlation function $g^{(2)} < 1$. In this way, the transition to PB is confirmed by the observation of the second-order correlation function that

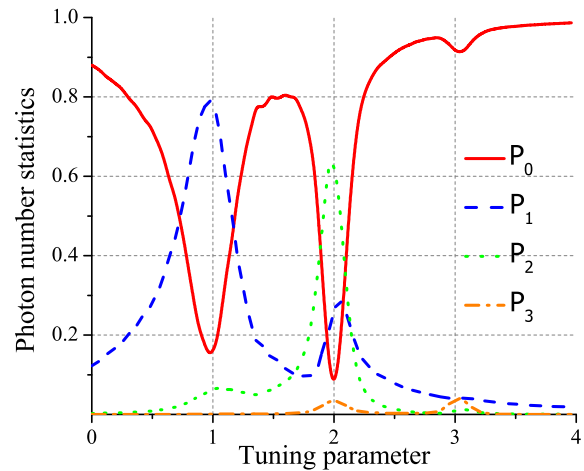


FIG. 8: The regimes of single-photon and two-photon blockades. The populations $P(n)$ for $n = 0, 1, 2, 3$, for time-intervals at the peak values of the mean photon numbers versus the tuning parameter. The parameters are: $\chi/\gamma = 30$, the maximum amplitude of pump field $\Omega/\gamma = 12$, the mean number of reservoir photons $N = 0.01$, $\tau = 5.5\gamma^{-1}$, $T = 0.4\gamma^{-1}$.

shows the transition from photon bunching to antibunching. The second-order correlation function versus the tuning parameter is plotted in Fig. 5(d). As calculations show, $g^{(2)} = 0.1$ for $k = 1$ in accordance with the result that for $|1\rangle$ Fock state the normalized second-order correlation function is zero. The correlation function displays the peak at $k = 1.6$. This result corresponds to the photon bunching with the level of mean photon number $\langle n \rangle = 0.38$. Then the second-order correlation function increases with increasing of the tuning parameter k , however, for negligible levels of the mean photon number.

B. Two-photon and three-photon blockades

In this subsection we analyse the multiphoton blockade on the base of photon-number effects. We will demonstrate how to chose the frequency of the driving field, the parameters of Gaussian pulses and the parameter of nonlinearity in order to realize effective populations of two-photon and three-photon states that indicate multiphoton blockades. It is obvious that for multiphoton blockade the regimes of photon state excitations with high levels of photon number in compared with the case of single-photon state excitation should be considered. Such regimes imply a larger peak strength of driving field or/and a comparative small nonlinear parameter. We present below the results for two possible operational regimes.

The typical results indicating the two-photon blockade are depicted in Fig. 7 and Fig. 8. The time evolution

of the mean photon number versus dimensionless time is depicted in Fig. 7(a) for the tuning parameter $k = 2$, (for the detuning $\Delta/\gamma = -\chi/\gamma$), corresponding to two-photon resonant excitation; the analogous result for one-photon excitation, $k = 1$, is shown in Fig. 7(b). This behavior repeats the periodicity of the driving pulses at the over transient regime. The analogous time-evolution is observed for the population P_2 at $k = 2$ (see, Fig. 7(c)). This regime is favorable for the selective excitation of two-photon number state, if the detuning $\Delta/\gamma = -\chi/\gamma$. In this case the population $P_2 = 0.61$ takes place due to two-photon excitation at the frequency $\omega_2 = \omega_0 + \chi$, for the tuning parameter $k = 2$ (see, Fig. 8), while the population of one-photon state has a comparative small value $P_1 = 0.28$. The peculiarity of this regime is that both one-photon blockade (for $k = 1$) and two-photon blockade (for $k = 2$) are effectively realized for the same parameters: $\chi/\gamma = 15$, $\Omega/\gamma = 6$, $\tau = 5.5\gamma^{-1}$, $T = 0.4\gamma^{-1}$. It should be mentioned that population P_2 comes over cw limit for the population of $|2\rangle$ Fock state and (that it is remarkable) for the population of $|1\rangle$ state in cw regime.

In Fig. 7(e) the normalized second-order correlation function versus dimensionless time is shown. The time-evolution involves photon correlation of thermal bath for time-interval that corresponds to resonator that involves only photon of thermal bath. Then, the peaks of $g^{(2)}$ take place at time-intervals at the front of pulses. Here quantum statistics is formed, but the mean photon number is negligible, therefore the peak in the correlation function is observed. At definite time intervals corresponding to peaked values of the mean photon number the correlation function equals to $g^{(2)} = 0.6$. These values of the correlation function are investigated in depending on the detuning (the parameter of tuning) and are shown in Fig. 7(f). As we see, for $k = 1$ the effective population of single-photon number state is observed, $P_1 = 0.79$ (see Fig. 8), and photon antibunching is realized $g^{(2)} = 0.6$. At $k = 2$, for which the maximal $P_2 = 0.61$ population is realized, the correlation function equals to $g^{(2)} = 0.6$ for the mean photon numbers $\langle n \rangle = 1.52$. Note, for the comparison that for $|2\rangle$ pure photon-number state the normalized second-order photon correlation function equals to 0.5. In this regime the photon bunching, $g^{(2)} = 2.2$, occurs for $k = 1.6$. In the vicinity of $k = 3$ the large level of $g^{(2)}$ is explained by the small level of the mean photon number (see, Fig. 9(a)).

In the end of this subsection we shortly discuss three-photon blockade. For observation of the selective excitation of three-photon states we need the operational regimes with more large levels of photon number than has been used for the previous cases. The typical results for this regime are plotted in Fig. 9 and Fig. 10. Time-evolution of the mean photon number versus dimensionless time is plotted in Fig. 9(a). This result shows the comparative large peak value of the mean photon number for the parameters $\chi/\gamma = 11$ and $\Omega/\gamma = 12$. In this case, Fig. 10 demonstrates large population $P_3 = 0.48$ of

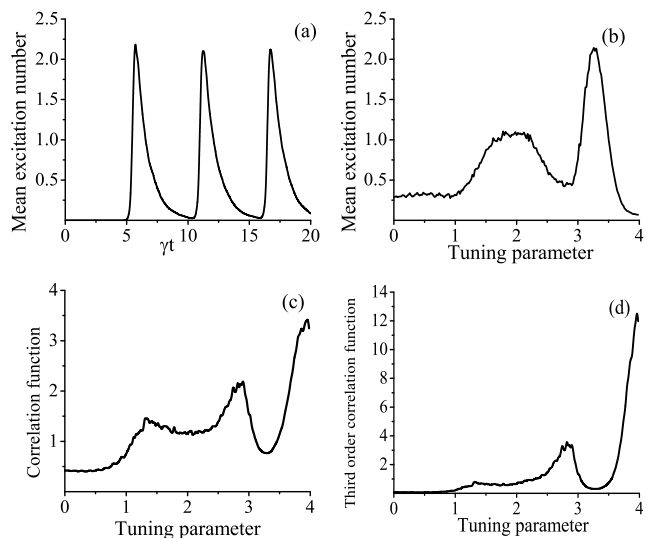


FIG. 9: The regime of three-photon blockades. The mean photon number versus dimensionless time, for $k = 3$ (a); the maximal peak values of the mean photon numbers depending on the tuning parameter (b); the second-order correlation function at the peak values of the mean photon numbers versus the tuning parameter (c); the third-order correlation function at the peak values of the mean photon numbers versus the tuning parameter (d). The parameters are: $\chi/\gamma = 11$, the maximum amplitude of pump field $\Omega/\gamma = 12$, the mean number of reservoir photons $N = 0.01$, $\tau = 5.5\gamma^{-1}$, $T = 0.4\gamma^{-1}$.

$|3\rangle$ Fock state for the tuning parameter $k = 3.28$. Thus, maximal population P_3 takes place for near to the resonance frequency $\omega = \omega_0 + 2.28\chi$.

The maximal values of the mean photon numbers for time-interval during pulses versus the tuning parameter are depicted in Fig. 9(b). This curve displays two-peak structure of the mean photon number. The first peak occurs at $k = 2$ which corresponds approximately to the mean photon number $\langle n \rangle = P_1 + 2P_2 + 3P_3 = 1.3$ in accordance with Fig. 8. The second characteristic double peak is at $k = 3.28$ and approximately equals to $\langle n \rangle = P_1 + 2P_2 + 3P_3 = 0.14 + 0.56 + 1.44$.

It is interesting to analyze selective excitation of three-photon state in the framework of the second-order and third-order correlation functions. The results of calculations are depicted in Fig. 9(c) and Fig. 9(d). As we see, for the case of the maximal population $P_3 = 0.48$ of $|3\rangle$ Fock state, if $k = 3.28$ and the mean photon number is $\langle n \rangle = 2$, the second-order correlation function is $g^{(2)} = 0.75$, (note, that for the pure $|3\rangle$ state $g^{(2)} = 2/3$ in accordance with the result obtained), while the third-order correlation function reaches to minimal value $g^{(3)} = 0.32$. It should be mentioned, that the last result is in accordance with the result for pure $|3\rangle$ Fock state, $g^{(3)} = 2/9$.

We emphasize that results of this subsection indicate the increasing of the populations of two-photon and

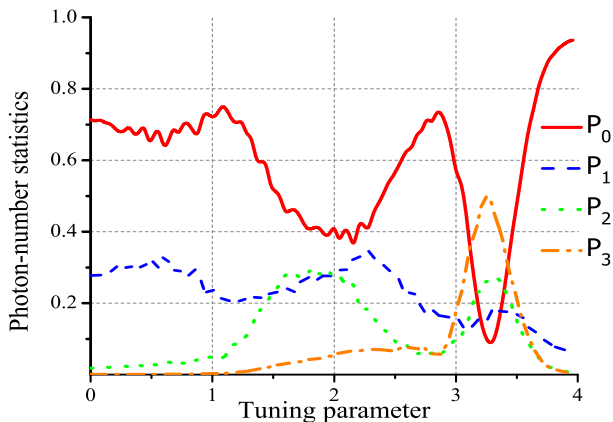


FIG. 10: The regime of three-photon blockades. The populations $P(n)$ for $n = 0, 1, 2, 3$, for time-intervals at the peak values of the mean photon numbers versus the tuning parameter. The parameters are: $\chi/\gamma = 11$, the maximum amplitude of pump field $\Omega/\gamma = 12$, the mean number of reservoir photons $N = 0.01$, $\tau = 5.5\gamma^{-1}$, $T = 0.4\gamma^{-1}$.

three-photon states of Kerr nonlinear resonator in the pulsed regime in comparison with the analogous results observed in the case of cw excitation (see, [16] and the results depicted in Fig. 3 and Fig. 4). This observation indicates on the efficiency of multiphoton blockades for the pulsed regimes.

IV. PRODUCTION OF MULTI-PHOTON STATES IN THE PULSED REGIMES

Recently, it has been demonstrated that formation of single-photon states can be realized in a cavity strongly coupled with emitter operated in the pulsed regime. In this way the photon-number effects and phase-space characteristics of photonic states can be controlled by choosing the parameters of driving pulses [26], [30]. In this section, we investigate production of two-photon and three-photon light states considering mainly the selectivity of the excitation of these states by driving pulses and their phase-space properties.

At first, we turn to the regime of single-photon blockade shown in Fig. 5 and Fig. 6 considering maximal values of the mean photon number for time-interval during pulses depending on the tuning parameter. The result of calculations are depicted in Fig. 11(a) where we plot the dependence of the mean photon number for different detunings. This curve shows a large spectral width of generation with the maximum at $\Delta = 0$. The peaked intensity is approximately $\langle n \rangle = P_1 + 2P_2 = 0.82 + 0.18$ with the populations have been obtained in Fig. 6.

Now, we consider production of two-photon states by selective two-photon excitations in Kerr nonlinear res-

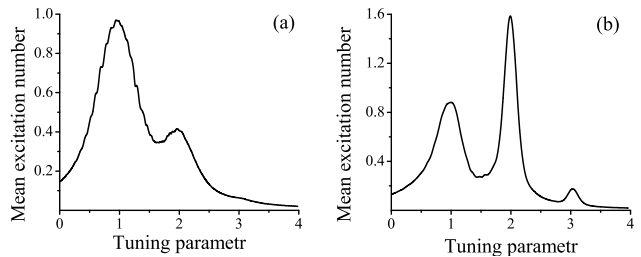


FIG. 11: The maximum values of the mean photon numbers depending on the tuning parameter. The parameters are: $\chi/\gamma = 15$, $\Omega/\gamma = 6$, $\tau = 5.5\gamma^{-1}$, $T = 0.4\gamma^{-1}$ (a); $\chi/\gamma = 30$, $\Omega/\gamma = 12$, $\tau = 5.5\gamma^{-1}$, $T = 0.4\gamma^{-1}$ (b). The mean number of reservoir photons $N = 0.01$.

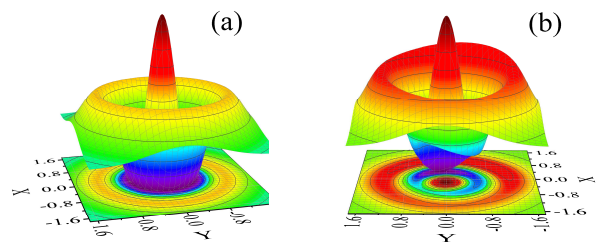


FIG. 12: The regime of selective two-photon excitation. The Wigner function for the pure $|2\rangle$ state (a); the Wigner function of cavity mode for time-interval corresponding to the maximal population of Fock state $|2\rangle$ (b). The negative regions of the Wigner functions are indicated in black. The parameters are: $\chi/\gamma = 15$, the maximum amplitude of pump field $\Omega/\gamma = 12$, the mean number of reservoir photons $N = 0.01$, $\tau = 5.5\gamma^{-1}$, $T = 0.4\gamma^{-1}$.

onator. In order to demonstrate the process we turn to the regime of two-photon blockade (see, the results depicted in Fig. 7 and Fig. 8). For these parameters the population of two-photon number state reaches $P_2 = 0.61$ for the detuning $\Delta/\gamma = -\chi/\gamma$. The curve of the maximal values of the mean photon numbers for these parameters are plotted in Fig. 11(b) in dependence from the detuning values. As we see, the mean photon number displays two-peak structure. The first peak occurs at $k = 1$ which corresponds approximately to the mean photon number $\langle n \rangle = P_1 + 2P_2 = 0.82 + 0.18$. The second characteristic double peak is at $k = 2$ and approximately equals to $\langle n \rangle = P_1 + 2P_2 = 0.3 + 1.22$.

To obtain a complete description of the system we turn to calculation of the Wigner function in phase-space. The numerical results are given for the regime used above that relies to effective selective excitation of two-photon states, for $k = 2$.

The Wigner function of intracavity mode for time-intervals corresponding to the maximal $P_2 = 0.61$ popu-

lation is shown in Fig. 12(b) with the Wigner function of pure $|2\rangle$ state, plotted in Fig. 12(a) for comparison. It is easy to realize that this Wigner function displays a ring signature with the center at $x = y = 0$ in the phase space and the good agreement in shape takes place with the Wigner function of pure $|2\rangle$ state.

Fig. 13 shows comparative analysis of the contour plots of the various Wigner functions corresponding to the definite detuning values that determine various resonant one-photon and multi-photon transitions. As we see, for the regime of one-photon excitation, $\Delta = 0$, on the frequency $\omega_1 = \omega_0$ the Wigner function (Fig. 13(a)) displays good agreement with the Wigner function of pure $|1\rangle$ single-photon state. In Fig. 13(b) the result for $k = 1.24$, i.e. for $\Delta/\gamma = -0.24\chi/\gamma$ is presented. In this case, the populations of vacuum state and single-photon state are crossing and are approximately equal (see, Fig. 8) thus, the Wigner function seems to be closest to the Wigner function of pure superposition state $|\Psi\rangle = \frac{1}{\sqrt{2}}(|0\rangle - |1\rangle)$. For $k = 2$, the contour plot depicted in Fig. 13(c) corresponds to the Wigner function of Fig. 12(b). In Fig. 13(d) the contour plot for the case of near the resonant three-photon excitation at $k = 3.28$ is depicted. This Wigner function shows three-phase symmetry and also indicates the regions of quantum interference in the contour plot as the negative regions in black. Note that three-fold symmetry of the Wigner function and interference pattern has been demonstrated for the direct three-photon down-conversion in $\chi^{(3)}$ media [42] and also in details for production of three-photon states in [43], [44].

V. CONCLUSION

We have investigated photon-number effects in multi-photon blockade for Kerr nonlinear dissipative resonator driven by sequence of Gaussian pulses. This model can be realized at least with two physical systems: a qubit off-resonantly coupled to a driven cavity or superconducting devices based on Josephson junction. We consider the cases of strong nonlinearity with respect to the rate of damping of the oscillatory mode. In these regimes the oscillatory energy levels are well resolved, and spectroscopic selective excitation of transitions between Fock states is possible by tuning the frequency of driving field.

Comparing the results for continuous wave- and pulsed- operational regimes of Kerr nonlinear resonator we demonstrate that the larger photon-number populations of the resonator can be reached if shaped pulses are implemented. Thus, we have shown that optimized one-photon and multi-photon blockades can be obtained by adequately choosing the duration of pulses and the time intervals between them.

Consideration of the Kerr nonlinear dissipative resonator under cw driving has been done on the framework of the potential solution of the Fokker-Planck equation for the quasiprobability distribution function in complex P-representation. In this way, we strongly demonstrated

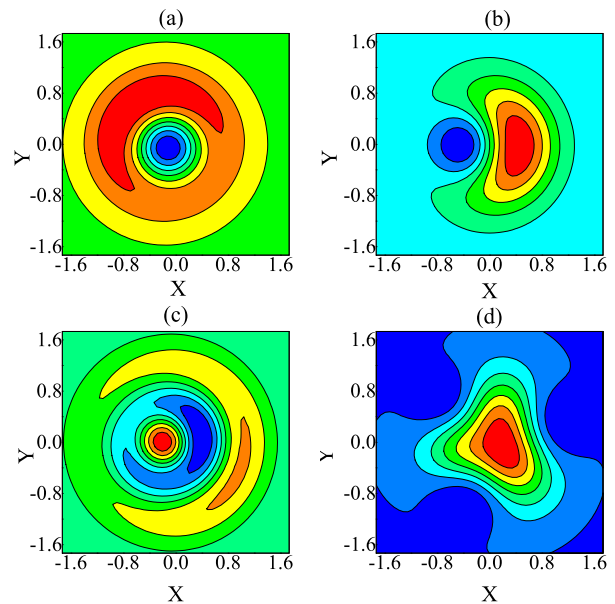


FIG. 13: The contour plots of the Wigner functions for the various selective excitations: $k = 1$ (a); $k = 1.24$ (b), where the populations of $|0\rangle$ and $|1\rangle$ are crossing each other (see, Fig. 8); $k = 2$ (c); $k = 3$ (d). The negative regions of the Wigner functions are indicated in black. The parameters are: $\chi/\gamma = 15$, the maximum amplitude of pump field $\Omega/\gamma = 12$, the mean number of reservoir photons $N = 0.01$, $\tau = 5.5\gamma^{-1}$, $T = 0.4\gamma^{-1}$.

that for the case of cw pumping of the Kerr-nonlinear resonator there are fundamental limits on the populations of lower photonic-number-states ($n=0, 1, 2, 3$). Particularly, the maximal value of $|1\rangle$ state population is limited by $P_1 = 0.5$ for all values of the system parameters.

More importantly, considering Kerr-nonlinear resonator driven by a sequence of Gaussian pulses, we have demonstrated the regimes in which the larger photon-number populations of the resonator beyond cw limits can be obtained. This improvement is due to a quantum control of decoherence in Kerr-nonlinear resonator by applying of suitable tailored e.g. pulses. Particularly, the typical results for P_1 population overcome 0.8 value.

We analyse photon-number effects and investigate in details the photon-number correlation effects on base of the second-order and third-order correlation functions for the case of selective excitations of intracavity mode. Specifically we have calculated the Wigner function in phase-space for the regimes of multi-photon excitations of mode.

Acknowledgments

We acknowledge support from the Armenian State Committee of Science, the Project No.13-1C031. G. Yu. K. acknowledges discussions with I. A. Shelykh.

-
- [1] A. Imamoglu, H. Schmidt, G. Woods, and M. Deutsch, *Phys. Rev. Lett.* **79**, 1467 (1997).
- [2] M. J. Werner and A. Imamoglu, *Phys. Rev. A* **61**, 011801(R) (1999).
- [3] K. M. Birnbaum et al., *Nature* 436, **87** (2005).
- [4] H. J. Carmichael, D.F. Walls, *J. Phys. B: Atom. Molec. Phys.* L43 **9** (1976) .
- [5] H. J. Kimble, M. Dagenais, L. Mandel, *Phys. Rev. Lett.* **39**, 691 (1977).
- [6] K. M. Birnbaum, A. Boca, R. Miller, A.D. Boozer, T. E. Northup, and H. J. Kimble, *Nature (London)* **436**, 87 (2005).
- [7] L. S. Bishop, J. M. Chow, J. Koch, A. A. Houck, M. H. Devoret, E. Thuneberg, S.M. Girvin, and R. J. Schoelkopf, *Nature Phys.* **5**, 105 (2008).
- [8] J. M. Fink, M. Goppl, M. Baur, R. Bianchetti, A. Leek, P. J. Blais, and A. Wallraf, *Nature (London)* **454**, 315 (2008).
- [9] A. Faraon, I. Fushman, D. Englund, N. Stoltz, P. Petro, and J. Vuckovic, *Nature Phys.* **4**, **859** (2008).
- [10] M. J. Hartmann, F. G. S. L. Brandao, and M. B. Plenio, *Laser Photon. Rev.* **2**, **527** (2008).
- [11] N. Na, S. Utsunomiya, L. Tian, and Y. Yamamoto, *Phys. Rev. A* **77**, 031803 (2008).
- [12] S. Schmidt and G. Blatter, *Phys. Rev. Lett.* **103**, 086403 (2009).
- [13] A. Tomadin, V. Giovannetti, R. Fazio, D. Gerace, I.Carusotto, H. E. Tureci, and A. Imamoglu, *Phys. Rev. A* **81**, 061801 (2010).
- [14] J. Q. Liao and C. K. Law, *Phys. Rev. A* **82**, 053836 (2010).
- [15] S. Ferretti, L. C. Andreani, H. E. Türeci, and D. Gerace, *Phys. Rev. A* **82**, 013841 (2010).
- [16] A. Miranowicz, M. Paprzycka, Y. X. Liu, J. Bajer, and F. Nori, *Phys. Rev. A* **87**, 023809 (2013).
- [17] L. Tian and H. J. Carmichael, *Phys. Rev. A* **46**, R6801 (1992).
- [18] A. J. Hoffman et al., *Phys. Rev. Lett.* **107**, 053602 (2011).
- [19] C. Lang et al., *Phys. Rev. Lett.* **106**, 243601 (2011).
- [20] A. Faraon, I. Fushman, D. Englund, N. Stoltz, P. Petroff, J. Vuckovic, *Nat. Phys.* **4**, 859 (2008).
- [21] P. Rabl, *Phys. Rev. Lett.* **107**, 063601 (2011).
- [22] A. Nunnenkamp, K. Børkje, and S. M. Girvin, *Phys. Rev. Lett.* **107**, 063602 (2011).
- [23] Y. X. Liu, A. Miranowicz, Y. B. Gao, J. Bajer, C. P. Sun, and F. Nori, *Phys. Rev. A* **82**, 032101 (2010).
- [24] A. Verger, C. Ciuti, and I. Carusotto, *Phys. Rev. B* **73**, 193306 (2006).
- [25] A. J. Hoffman, S. J. Srinivasan, S. Schmidt, L. Spietz, J. Aumentado, H. E. Tureci, and A. A. Houck, *Phys. Rev. Lett.* **107**, 053602 (2011).
- [26] A. Faraon, A. Majumdar, and J. Vuckovic, *Phys. Rev. A* **81**, 033838 (2010).
- [27] H. H. Adamyany and G. Yu. Kryuchkyan, *Phys. Rev. A* **74**, 023810 (2006).
- [28] N. H. Adamyany, H. H. Adamyany, and G. Yu. Kryuchkyan, *Phys. Rev. A* **77**, 023820 (2008).
- [29] T. V. Gevorgyan, A. R. Shahinyan, and G. Yu. Kryuchkyan, *Phys. Rev. A* **79**, 053828 (2009).
- [30] T. V. Gevorgyan, A. R. Shahinyan, and G. Yu. Kryuchkyan, *Phys. Rev. A* **85**, 053802 (2012).
- [31] T. V. Gevorgyan, A. R. Shahinyan, Lock Yue Chew and G. Yu. Kryuchkyan, *Phys. Rev. E* **88**, 022910 (2013).
- [32] T. V. Gevorgyan and G. Yu. Kryuchkyan, *Journal of Modern Optics* **60**, 860 (2013).
- [33] J. Atalaya, A. Isacson, and M. I. Dykman, *Phys. Rev. Lett.* **106**, 2272702 (2011).
- [34] M. I. Dykman and D. Ryvkine, *Phys. Rev. Lett.* **94**, 070602 (2011).
- [35] M. I. Dykman, M. Marthaler, and V. Peano, *Phys. Rev. A* **83**, 052115 (2011).
- [36] D. Ryvkine and M. I. Dykman, *Phys. Rev. E* **73**, 061109 (2006).
- [37] A. Miranowicz, W. Leóński, *J. Opt. B: Quantum Semi-class. Opt.***6**, 943-946 (2004).
- [38] P. D. Drummond and D. F. Walls 1980 *J. Phys. A: Math. Gen.* **13**, 725 (1980).
- [39] G. Yu. Kryuchkyan and K. V. Kheruntsyan, *Opt. Comm.*,**120**, 132 (1996).
- [40] K. V. Kheruntsyan, et al., *Opt. Comm.* **139**, 157 (1997).
- [41] K. V. Kherunstyan, *J. Opt. B: Quantum Simclassical Opt.*,**1**, 225 (1999).
- [42] K. Banaszek and P. L. Knight, *Phys. Rev. A* **55**, 2368 (1997).
- [43] G. Yu. Kryuchkyan and N. T. Muradyan, *Phys. Lett. A* 286, 113 **286**, 113 (2001).
- [44] D. A. Antonosyan, T. V. Gevorgyan and G. Yu. Kryuchkyan, *Phys. Rev. A*, **83**, 043807 (2011).